Available online at www.sciencedirect.com
ScienceDirect
Journal of Catalysis 250 (2007) 75–84
JOURNAL OF CATALYSIS
www.elsevier.com/locate/jcat

# Comparison of the catalytic activity of $MO_2$ (M = Ti, Zr, Ce) for soot oxidation under $NO_x/O_2$

I. Atribak, I. Such-Basáñez, A. Bueno-López *, A. García-García

*Department of Inorganic Chemistry, University of Alicante, Ap. 99, E-03080 Alicante, Spain*

Received 15 March 2007; revised 9 May 2007; accepted 20 May 2007

Available online 29 June 2007

**Abstract**

The catalytic activity of $TiO_2$, $ZrO_2$, and $CeO_2$ for soot oxidation under $NO_x/O_2$ was compared. Characterisation of the oxides by $N_2$ adsorption at −196 °C, Raman spectroscopy, and XRD revealed that the predominant crystalline phase of $TiO_2$ (rutile or anatase) and $ZrO_2$ (monoclinic or tetragonal) had no significant affect on the catalytic activity of these oxides for soot oxidation with $NO_x/O_2$. $CeO_2$, with the only allowed fluorite structure, is the most active oxide because accelerates the NO conversion to $NO_2$, whereas $TiO_2$ and $ZrO_2$ do not catalyse this reaction. Once $NO_2$ is produced by $CeO_2$, part of it reacts with soot, and a certain amount is stored on $CeO_2$. $NO_x$ stored on $CeO_2$ under reaction conditions (around 450 °C) does not accelerate soot oxidation and can be evolved under $N_2$ flow but not under a $NO_x/O_2$ stream. $NO_x$ storage on $TiO_2$ and $ZrO_2$ under reaction conditions was not detected. An additional benefit of $CeO_2$ with regard to $TiO_2$ and $ZrO_2$ is that the $CeO_2$-catalysed soot oxidation yields mainly $CO_2$, whereas $TiO_2$ and $ZrO_2$ yield higher percentages of CO. This can be attributed to the lowest $CeO_2$-catalysed soot oxidation temperature and to the ability of $CeO_2$ to catalyse CO oxidation to $CO_2$. The effect of thermal sintering at 800 °C (decreased BET surface area and increased crystal size) on $CeO_2$ is more important than on $TiO_2$ and $ZrO_2$, but 800 °C-calcined $CeO_2$ is still more active for soot combustion than the other oxides studied.


*Keywords:* Diesel exhausts; Soot; Metal oxide catalyst; $CeO_2$; $TiO_2$; $ZrO_2$; $NO_x$

## 1. Introduction

Vehicles used in heavy-duty applications incorporate diesel engines. This includes buses, large trucks, and off-highway construction mining equipment. Furthermore, diesel engines are winning an increasing share of the worldwide light-duty vehicle market [1]. Currently in Europe, about 100% of heavy duty, 60% of light-duty commercial vehicles, and 20% of passenger cars are diesel-powered. The popularity of the diesel engine revolves around its fuel efficiency, reliability, and durability. The high compression ratios and relatively high $O_2$ concentrations in the diesel combustion chambers are responsible for the better fuel efficiency and lower CO and hydrocarbon emissions compared with a gasoline engine [2]. However, these same factors result in higher $NO_x$ emissions [3] and emanation of particulate matter comprised primarily of carbon, on which heavy hydrocarbons, sulfates, and water are adsorbed. $NO_x$ and particular matter have been linked to serious environmental and health problems.

Because the $NO_x$ and particulate emissions cannot be avoided by engine modifications alone, postcombustion catalytic processes for reducing the emission of both harmful substances must be developed. Selective catalytic reduction (SCR) and $NO_x$-storage catalysts have been proposed for $NO_x$ reduction. Catalytic regeneration of diesel particulate filters for soot removal is also promising. A number of catalysts have been investigated for pollution control in diesel exhausts, including Pt [4], molten salts [5], perovskites [6], and different metal oxides [7,8] among others.

A soot oxidation catalyst (SOC) usually combines highly active metals or metal oxides with different supports, including

* Corresponding author. Fax: +34 965 90 34 54.
*E-mail address:* agus@ua.es (A. Bueno-López).

0021-9517/$ – see front matter 
doi:10.1016/j.jcat.2007.05.015

zeolites and metal oxides, among others. In many cases, the role of the support in the catalytic activity of the metal is crucial. For example, Oi-Uchisawa et al. [9] studied soot oxidation under simulated diesel exhaust conditions with Pt supported on different oxides and found that activity decreased in the order $Ta_2O_5 > Nb_2O_5 \approx WO_3 \approx SnO_2 \approx SiO_2 > TiO_2 > Al_2O_3 \approx ZrO_2$. Pt supported on zeolites (Na-Y, Ba-Y, Ferrierite, ZSM-22, ETS-10, and AlPO-11), $Al_2O_3$, and $TiO_2$ were also tested for soot oxidation under simulated diesel exhaust conditions, and a significant effect of the support also was reported in this case [10]. Neeft et al. [11] studied catalysed soot oxidation by $O_2$ with two catalysts containing a mixture of metals [Cu/K/Mo/(Cl)] supported on $TiO_2$ and $ZrO_2$, respectively, the former being more active than the latter, and Braun et al. [12] demonstrated that $Mo/SiO_2$ is more active than $Mo/TiO_2$ for soot oxidation in air.

On the other hand, the role of the support in catalysts is also crucial to $NO_x$ removal. Recently, a series of $Pt/MO_2$ and Pt–$Ba/MO_2$ (M = Ce, Si, Zr) catalysts was investigated in terms of $NO_x$ storage and subsequent reduction of the stored $NO_x$ species by propene. Among the Ba-free catalysts, $Pt/CeO_2$ exhibited the highest $NO_x$ uptake, whereas $Pt/SiO_2$ demonstrated no $NO_x$ uptake [13]. A study of the chemisorptive properties of $Pt/Al_2O_3$, $Pt/CeO_2$, and $Pt/ZrO_2$ catalysts and of the bare supports toward NO and propylene concluded that the relative population and thermal stability of adsorbed $NO_x$ species depended on the nature of the metal oxide used as the support [14]. $Pt/ZrO_2$ promotes NO dissociation and nitrite/nitrate decomposition at lower temperatures compared with $Pt/Al_2O_3$ and $Pt/CeO_2$ catalysts. Investigation of the catalytic performance of the three catalysts for the SCR of NO by propylene revealed that the $Pt/ZrO_2$ catalyst was much more active than $Pt/CeO_2$, with $Pt/Al_2O_3$ exhibiting an intermediate performance [14].

But despite the decisive role of the supports demonstrated in many cases, few studies have focused on comparisons of catalytic activity of single oxides for soot oxidation under diesel exhaust conditions. Van Doorn et al. [15] studied the catalytic role of several metal oxides in soot combustion by $O_2$ and concluded that $Al_2O_3$ and $SiO_2$ had no catalytic effect; $TiO_2$ and $ZrO_2$ had moderate activity, and $CeO_2$, $La_2O_2CO_3$, and $V_2O_5$ exhibited substantial activity for soot combustion. Numerous metal oxide catalysts for soot oxidation by $O_2$ were also screened by Neeft et al. [16], but those studies were carried out without $NO_x$ in the gas mixture, and thus the conclusions cannot be directly extrapolated to diesel exhaust conditions.

Considering these premises, the aim of the present study was to compare the catalytic activity for soot oxidation under $NO_x/O_2$ of three metal oxides ($TiO_2$, $ZrO_2$, and $CeO_2$) commonly used as catalyst supports and even as catalysts in some cases. These oxides were selected because they present different activities for soot oxidation, with $CeO_2$ the most active oxide and $ZrO_2$ the least active oxide considering the studies noted in this section [9,11]. Taking into account the highest activity of $CeO_2$, special attention was paid to the behaviour of this oxide.

## 2. Experimental

### 2.1. Catalyst preparation

$CeO_2$ and $ZrO_2$ samples were prepared by precipitation of the corresponding hydroxides (at pH 9) from aqueous solutions of $Ce(NO_3)_3{\cdot}6H_2O$ and $ZrO(NO_3)_2{\cdot}6H_2O$, respectively (precursors provided by Aldrich, 99.9% purity), by dropping a diluted water solution of $NH_3$. The hydroxides were dried in air at 110 °C overnight and further calcinated at 600 or 800 °C for 2 h. $TiO_2$ samples were prepared by thermal treatment of $TiO_2$ (P25, Degussa) in air for 2 h at the same temperatures. The samples are designated $MO_2$-$T^a$, where M = Ti, Zr, or Ce and $T^a = 600$ or 800 °C.

### 2.2. Catalyst characterisation

BET surface area of samples was determined by physical adsorption of $N_2$ at −196 °C in an automatic volumetric system (Autosorb-6B, Quantachrome) after degassing at 250 °C for 4 h. Raman spectra were recorded in a LabRam Jobin-Yvon (Horiba) spectrograph coupled to a microscope. A He/Ne laser ($\lambda = 632.82$ nm) source was used as the light source, and a Perltier cooled CCd served as the detector. A power of approximately 0.9 mW reached the sample through a ×50 VLWD ($n/a = 0.50$) objective for 3 s, and 15 consecutive spectra were added to obtain the final spectrum. Several expressions have been proposed to estimate the ratio of tetragonal and monoclinic phases in $ZrO_2$ samples, relying on the bands at 148, 267 $cm^{-1}$ (tetragonal only), and the doublet at 180–190 $cm^{-1}$ (due to monoclinic only) [17–19]. The most commonly used expression, and also the one used in this study, is

$$F_t = 0.97\big(I_t(148\ \mathrm{cm}^{-1}) + I_t(267\ \mathrm{cm}^{-1})\big) \times \big(I_t(148\ \mathrm{cm}^{-1}) + I_t(267\ \mathrm{cm}^{-1}) + I_m(180\ \mathrm{cm}^{-1}) + I_m(190\ \mathrm{cm}^{-1})\big)^{-1} \quad (1)$$

where $I_i$ is taken to be the integral intensity of the band and no polarization effects are considered [19–21].

X-ray diffractograms were measured on a Seifert powder diffractometer using the Cu$K_\alpha$ radiation ($\lambda = 0.15418$ nm). Spectra were recorded between 10° and 60° ($2\theta$) with a step size of 0.05 and measuring for 3 s at each step. From XRD data, different phases of the studied compounds were identified and quantified. Phase composition on $TiO_2$ samples was calculated using

$$F_R = \frac{1.26 I_R(110)}{I_A(101) + 1.26 I_R(110)} \quad (2)$$

where $F_R$ is the rutile fraction, $I_A(101)$ is the intensity of the most intense anatase peak, and $I_R(110)$ is the intensity of the most intense rutile peak [22,23].

Phase composition determination of $ZrO_2$ samples was performed in a similar manner, and the following equation presents the expression to calculate the fraction of tetragonal phase from XRD patterns:

$$F_t = \frac{I_t(111)}{I_t(111) + I_m(-111) + I_m(111)} \quad (3)$$

where $F_t$ is the tetragonal fraction, $I_t(111)$ is the intensity of the tetragonal peak (111), and $I_m(-111)$ and $I_m(111)$ are the intensities of the monoclinic peaks (−111) and (111), respectively.

The crystal sizes ($D$) of all the phases present in the catalysts were estimated using Scherrer's equation

$$D = \frac{K\lambda}{\beta \cos\theta} \quad (4)$$

where $\lambda$ is the wavelength of the radiation used (Cu$K_\alpha$), $\beta$ is the full width at half maximum of the diffraction peak considered, $K$ is a shape factor taken as 0.9 (1 being a perfect sphere), and $\theta$ is the diffraction angle at which the peak appears.

### 2.3. Catalytic activity

Reactivity tests were carried out at atmospheric pressure in a cylindrical fixed-bed reactor (1 cm of inner diameter) connected to specific NDIR-UV gas analysers for NO, $NO_2$, CO, $CO_2$, and $O_2$ (Fisher–Rosemount, models BINOS 1004, 100 and 1001). Soot-catalysts mixtures (80 mg of catalyst + 20 mg of soot) were prepared in loose contact [11] and diluted with 350 mg of SiC. The addition of SiC decreases the flow resistance of the sample bed and provides a heat sink, which decreases temperature gradients in the sample. The reactive gas mixtures used (500 ml/min, GHSV ∼30,000 $h^{-1}$) contained 0.05% $NO_x$ + 5% $O_2$ + balance $N_2$ or 5% $O_2$ + balance $N_2$. Temperature-programmed reactions (TPRs) were performed by raising the temperature from 25 to 700 °C at a rate of 10 °C/min. In addition, isothermal reactions at 450 °C were carried out, consisting of heating the sample from room temperature up to 450 °C under $N_2$ flow, after which the inert gas was replaced by the reactive mixture. Isothermal reactions were conducted until the constant level of the different gases was reached.

Soot conversion profiles were determined from the CO and $CO_2$ evolved, and the selectivity of the different catalysts for CO emission was determined using

$$CO/CO_x\ (\%) = 100CO/(CO + CO_2). \quad (5)$$

Blank experiments were also performed under the aforementioned experimental conditions but without soot, that is, using only the catalyst.

In addition, TPRs were performed with selected catalysts under the described conditions but following the gas composition with a gas chromatograph (HP model 6890 Plus Series) equipped with a switched dual-column system and two serial columns (a Porapak Q 80/100 for $CO_2$ and $N_2O$ separation and a Molecular Sieve 13X for $O_2$, $N_2$, and CO separation) and a Chemiluminiscence $NO_x$ analyser for NO and $NO_2$ analysis (SIGNAL 400VM).

The model soot used in this study was carbon black from Degussa S.A. (Printex-U), with 92.2% C, 0.6% H, 0.2% N, and 0.4% S. The ash and adsorbed hydrocarbon percentages were <0.1 and 5.2%, respectively, and the BET surface area was 95 $m^2/g$.

## 3. Results

### 3.1. Characterization of materials

BET surface areas of the samples used in this study are displayed in Table 1. $TiO_2$-600 and $ZrO_2$-600 had the same BET area (47 $m^2/g$), with $CeO_2$-600 exhibiting a lower value (37 $m^2/g$). As expected, the samples calcined at 800 °C had lower surface area values than those samples calcined at 600 °C due to sintering. Calcination temperature had a greater effect on $CeO_2$ compared with $TiO_2$ and $ZrO_2$; 84% of the area of $CeO_2$ was lost when calcined at 800 °C compared with that at 600 °C, with comparable values of 57% for $ZrO_2$ and 66% for $TiO_2$.

All samples were characterised by Raman spectroscopy; the data are collected in Fig. 1. Raman spectra of $TiO_2$ calcined at 600 and 800 °C are shown in Fig. 1a. $TiO_2$ is known to appear mainly in two different crystal structures (besides brookite): rutile and anatase (designated R and A in Fig. 1a). The Raman spectrum of $TiO_2$ calcined at 800 °C was consistent with the spectrum of pure rutile, even though the presence of anatase cannot be ruled out. $TiO_2$-800 showed bands at 142, 235, 446, and 608 $cm^{-1}$. The bands at 142, 446, and 608 $cm^{-1}$ can be assigned to the $B_{1g}$, $E_g$, and $A_{1g}$ modes of rutile, respectively [24,25]. The broad band at 234 $cm^{-1}$ has been identified as a second-order phonon that disappears at low temperature [26]. The spectrum of $TiO_2$-600 presented bands at 144, 394, 517, and 637 $cm^{-1}$, which can be assigned to $E_g$, $B_{1g}$, $A_{1g}$, and $E_g$ of anatase, respectively [27]. $TiO_2$-600 also presented features of the Raman spectrum of rutile appearing as shoulders at 446 and 607 $cm^{-1}$, indicating a mixture of both rutile and anatase phases on sample $TiO_2$-600, even though estimating phase proportion by Raman spectroscopy for these materials is not straightforward.

The Raman spectra of zirconia samples calcined at 600 and 800 °C is shown in Fig. 1b. When $ZrO_2$ is synthesised by a pre-

Table 1
Phase composition, crystal sizes, and BET surface area of the catalysts

| Sample | Phase (fraction)/particle size (nm) | $S_{BET}$ ($m^2/g$) |
|---|---|---|
| $TiO_2$-600 | Rutile (0.36)/32; Anatase (0.64)/21 | 47 |
| $TiO_2$-800 | Rutile (1)/45 | 16 |
| $ZrO_2$-600 | Tetragonal (0.56[a]; 0.50[b])/13; Monoclinic (0.44[a]; 0.50[b])/11 | 47 |
| $ZrO_2$-800 | Tetragonal (0.24[a]; 0.22[b])/17; Monoclinic (0.76[a]; 0.78[b])/15 | 20 |
| $CeO_2$-600 | Fluorite (1)/18 | 37 |
| $CeO_2$-800 | Fluorite (1)/39 | 6 |

[a] Phase fraction calculated by XRD.
[b] Phase fraction calculated by Raman spectroscopy.

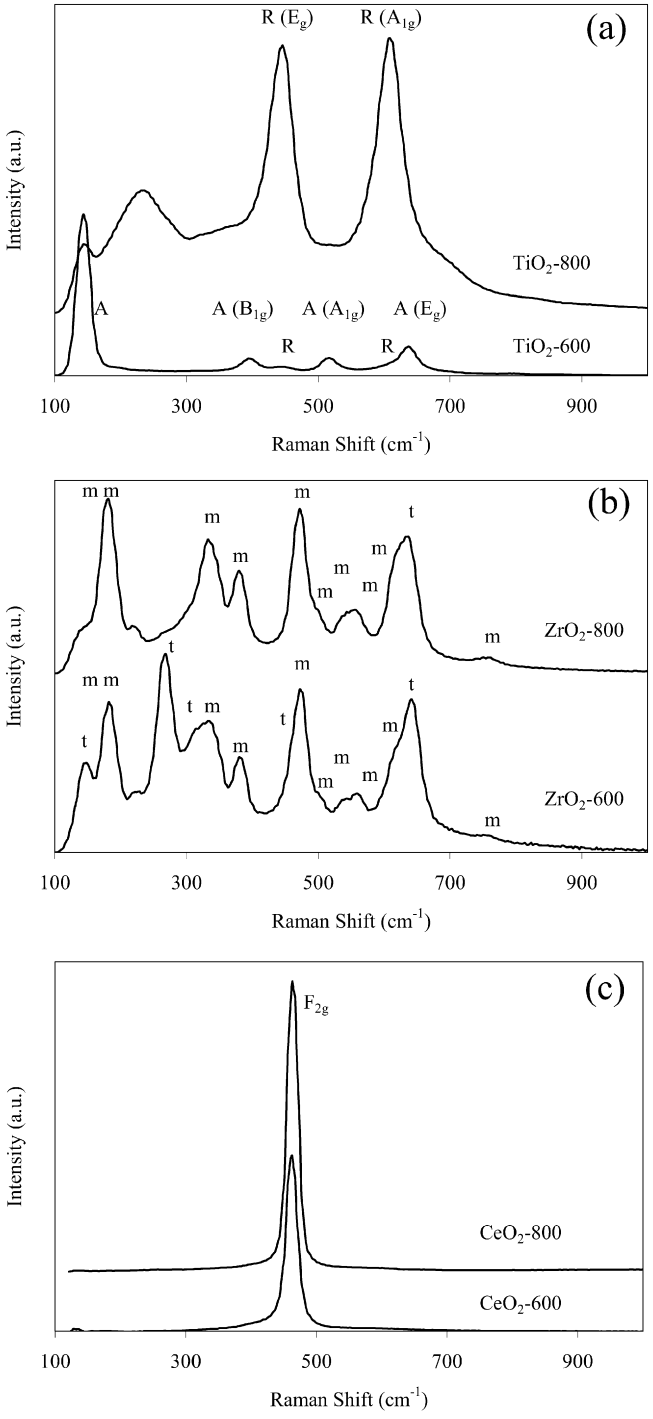


Fig. 1. Raman spectra of (a) $TiO_2$, (b) $ZrO_2$, and (c) $CeO_2$ catalysts.

cipitation route, the predominant phase will be monoclinic or tetragonal, depending on calcinations conditions (mainly temperature, time, and atmosphere) [28]. It is quite common to obtain materials in which a mixture of monoclinic and tetragonal phases appears. The Raman spectra of $ZrO_2$ shown in this paper exhibit features of both monoclinic and tetragonal phases ($m$ and $t$, respectively, in Fig. 1b). The tetragonal phase is characterized by six Raman active modes ($D_{4h}^{15}$, $A_{1g}+2B_{1g}+3E_g$), whereas for the monoclinic phase ($C_{2h}^{5}$), 18 active Raman modes are expected from symmetry analysis [29].

Tetragonal zirconia presented bands at 148, 267, 322, 464, and 648 $cm^{-1}$. Some of these bands were unique, but most of them overlapped significantly with bands due to the monoclinic phase of zirconia, which presented bands a doublet at 180 and 190, 333, 380, 475, 502, a doublet at 539 and 559, 618, and 757 $cm^{-1}$, some of which are not resolved in Fig. 1b due to the analysis conditions used. The values obtained for the fraction of tetragonal and monoclinic phase, along with those obtained by XRD, are summarized in Table 1.

The samples of $CeO_2$ calcined at 600 and 800 °C (Fig. 1c) presented a Raman characteristic band at about 465 $cm^{-1}$, which can be unambiguously assigned to the $F_{2g}$ mode of fluorite-type structures [30–32]. Band position did not change when calcination temperature was modified; however, an increase in the calcination temperature produced a significant increase in the intensity of the $F_{2g}$ band and narrowing of the band. Thus, increased crystallinity of the material with increasing calcination temperature can be inferred.

Samples were also characterized by XRD; Fig. 2 collects XRD patterns of all of the materials used in this study. XRD patterns of $TiO_2$ calcined at 600 and 800 °C are shown in Fig. 2a. Sample $TiO_2$-600 comprised a mixture of anatase and rutile phases, whereas $TiO_2$-800 did not show the main features of anatase [$A(101)$ and $A(200)$]. These results are congruent with the observations from the Raman spectra of $TiO_2$-600 and $TiO_2$-800. The results of phase composition analysis, together with crystal size of each phase [calculated from Scherrer's equation, using $R(110)$ and $A(101)$ peaks] are compiled in Table 1. Narrower rutile peaks can be seen at higher calcination temperatures, and thus an increase in crystallite size can be deduced.

XRD diffractograms of zirconia samples show that both samples used in this study are mixtures of monoclinic and tetragonal phases. The most important features of the diffractogram are seen between 20° and 40° ($2\theta$), with two intense peaks [$m(-111)$ and $m(111)$] due to the monoclinic phase and one intense peak due to the tetragonal phase [$t(111)$]. From Fig. 2b, it can be concluded that at the higher calcination temperature ($ZrO_2$-800), monoclinic phase was slightly more abundant than tetragonal phase, whereas the opposite situation was encountered at the lower temperature ($ZrO_2$-600). As in the case of $TiO_2$, peaks corresponding to the monoclinic phase of $ZrO_2$ calcined at 800 °C were narrower, and, as shown in Table 1, crystal sizes were larger.

XRD analysis of $CeO_2$ is shown in Fig. 2c. No other phase than ceria with a fluorite-type structure was detected; however, crystal size changes can be seen in the diffractograms, with narrower peaks in $CeO_2$-800 compared with those in $CeO_2$-600 are. Data on crystal size are compiled in Table 1. In general, increased calcination temperature led to a significant drop in the surface area of $CeO_2$ and a consequent increase in crystal size (54%).

### 3.2. Catalytic activity

Fig. 3 shows the soot conversion profiles obtained in TPRs performed with $TiO_2$, $ZrO_2$, and $CeO_2$ catalysts under $NO_x/O_2$,

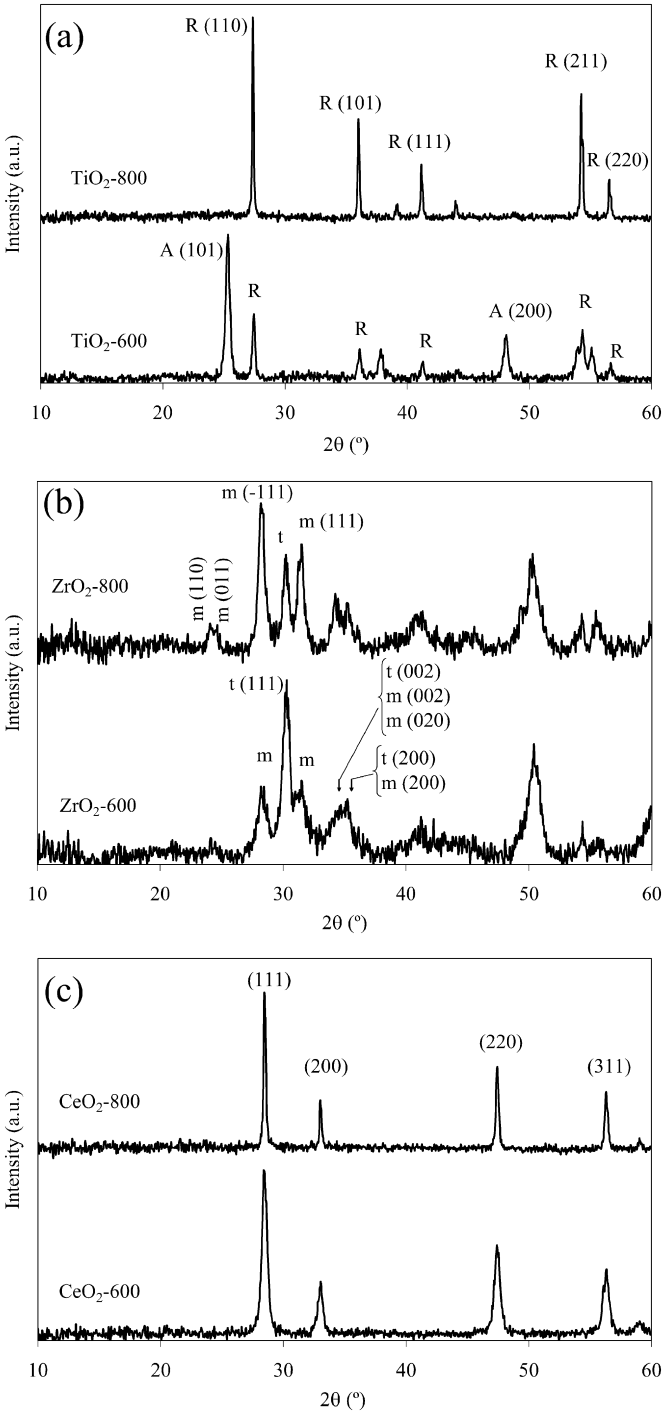


Fig. 2. XRD patterns of (a) $TiO_2$, (b) $ZrO_2$, and (c) $CeO_2$ catalysts.

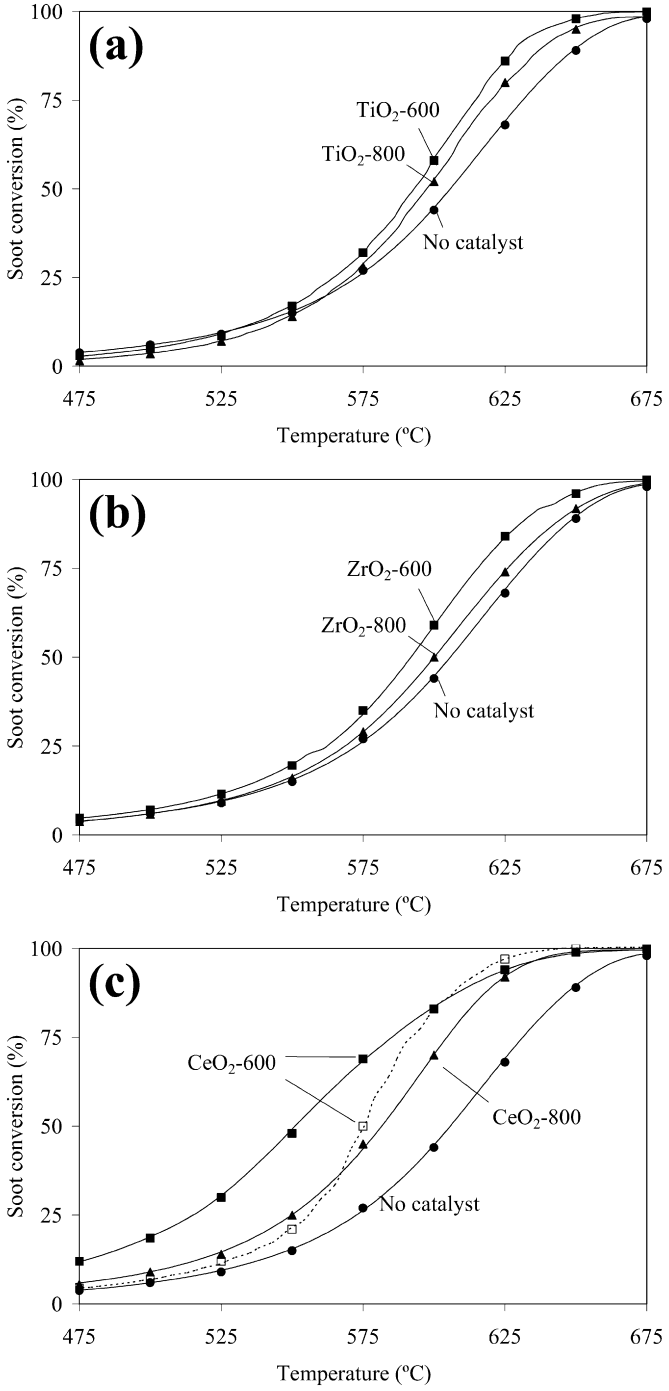


Fig. 3. Soot conversion in temperature programmed reactions under $NO_x/O_2$ (solid symbols) with different catalysts. (a) $TiO_2$, (b) $ZrO_2$, and (c) $CeO_2$. (The experiment represented by open symbols was carried out under $O_2$.)

along with the profile of the uncatalysed reaction. The corresponding temperatures for 50% soot conversion ($T_{50\%}$) are included in Table 2. All of the metal oxides tested decreased the soot oxidation temperature, with differences among them observed. $CeO_2$ catalysts were more active than their counterpart $ZrO_2$ and $TiO_2$ catalysts, and in general, catalysts calcined at 600 °C were more active than those calcined at 800 °C. The most active catalyst, $CeO_2$-600, lowered the $T_{50\%}$ parameter at 55 °C with regard to the uncatalysed reaction. The catalytic activity of $CeO_2$-600 also was checked under $O_2$ (Fig. 3c); despite exhibiting less activity for soot oxidation than under $NO_x/O_2$ atmosphere, significant activity was maintained. The high activity of $CeO_2$ for soot combustion with $O_2$ was attributed to the production of active oxygen, that is, gas-phase $O_2$ was incorporated to the $CeO_2$ lattice, and atomic oxygen from the lattice was delivered to soot [7,8]. However, in the presence of $NO_x$, additional factors play important roles, as we discuss next.

The analysis of the CO and $CO_2$ emission during the TPRs provides complementary information. From a practical stand-

Table 2
Temperature for 50% soot conversion ($T_{50\%}$) and selectivity to CO (determined with Eq. (5)) in temperature programmed reactions performed under $NO_x/O_2$

| Sample | $T_{50\%}$ (°C) | $CO/CO_x$ (%) |
|---|---|---|
| $TiO_2$-600 | 593 | 56.6 |
| $TiO_2$-800 | 598 | 60.2 |
| $ZrO_2$-600 | 592 | 43.4 |
| $ZrO_2$-800 | 600 | 62.6 |
| $CeO_2$-600 | 551 | 15.2 |
| $CeO_2$-800 | 581 | 67.5 |
| Uncatalysed | 606 | 65.5 |

point, $CO_2$ formation is preferable due to the high CO toxicity. The percentages of CO emitted during the TPRs performed under $NO_x/O_2$ were calculated according to Eq. (5) and are included in Table 2. The uncatalysed carbon gasification yielded both CO and $CO_2$, with CO the most abundant component (65.5%). All of the catalysts calcined at 600 °C decreased CO formation, and among these, $CeO_2$-600 yielded the lowest amount of CO. In contrast, the catalysts calcined at 800 °C hardly improved $CO_2$ formation with regard to CO.

$NO_x$ elimination profiles obtained with the series of catalysts studied are given in Fig. 4. Most of the catalysts exhibited a single band, and the temperatures of maximum $NO_x$ elimination and of the onset of $NO_x$ elimination corresponding to catalysed reactions decreased with regard to those for uncatalysed reactions. The sample $CeO_2$-600 showed unique behaviour; the $NO_x$ elimination profile obtained with this catalyst was complex and ranged from approximately 225 °C to above 700 °C. This broad profile suggests that several processes are occurring, as we discuss later.

Considering the temperatures of maximum $NO_x$ elimination with the series of oxides calcined at 600 or 800 °C, the activity for $NO_x$ elimination increases in the order $ZrO_2 \leqslant TiO_2 < CeO_2$, in agreement with the trend of activity for soot oxidation deduced from Fig. 3 and from the $T_{50\%}$ values included in Table 2.

$O_2$ conversion profiles corresponding to selected TPRs performed under $NO_x/O_2$ are plotted in Fig. 4 together with those of $NO_x$ elimination. Fig. 4a shows quite parallel $NO_x$ and $O_2$ elimination profiles during the $TiO_2$-600-catalysed reaction, with the $NO_x$ elimination onset temperature slightly lower than the $O_2$ elimination onset temperature. Quite similar behaviour can be observed for the catalyst $ZrO_2$-600 shown in Fig. 4b; that is, the $NO_x$ and $O_2$ elimination profiles are concurrent. This type of behaviour, with parallel $O_2$ and $NO_x$ elimination curves, was also observed in the reactions performed with all of the catalysts calcined at 800 °C ($O_2$ profiles not included for brevity). This suggests that in all of these experiments, $NO_x$ and $O_2$ were consumed due to reduction with soot once the reaction temperature for its gasification was achieved. The $NO_x$ elimination profiles obtained with $TiO_2$-600 and $ZrO_2$-600 were slightly different, whereas the soot conversion profiles (Fig. 3) corresponding to these experiments were very similar. In the experiment performed with $TiO_2$-600, $NO_x$ elimination at ca. 450–500 °C was higher than that using $ZrO_2$-600 as a catalyst, suggesting that $TiO_2$-600 is slightly more selective toward $NO_x$ reduction with regard to $O_2$ combustion than $ZrO_2$-600 in this temperature range.

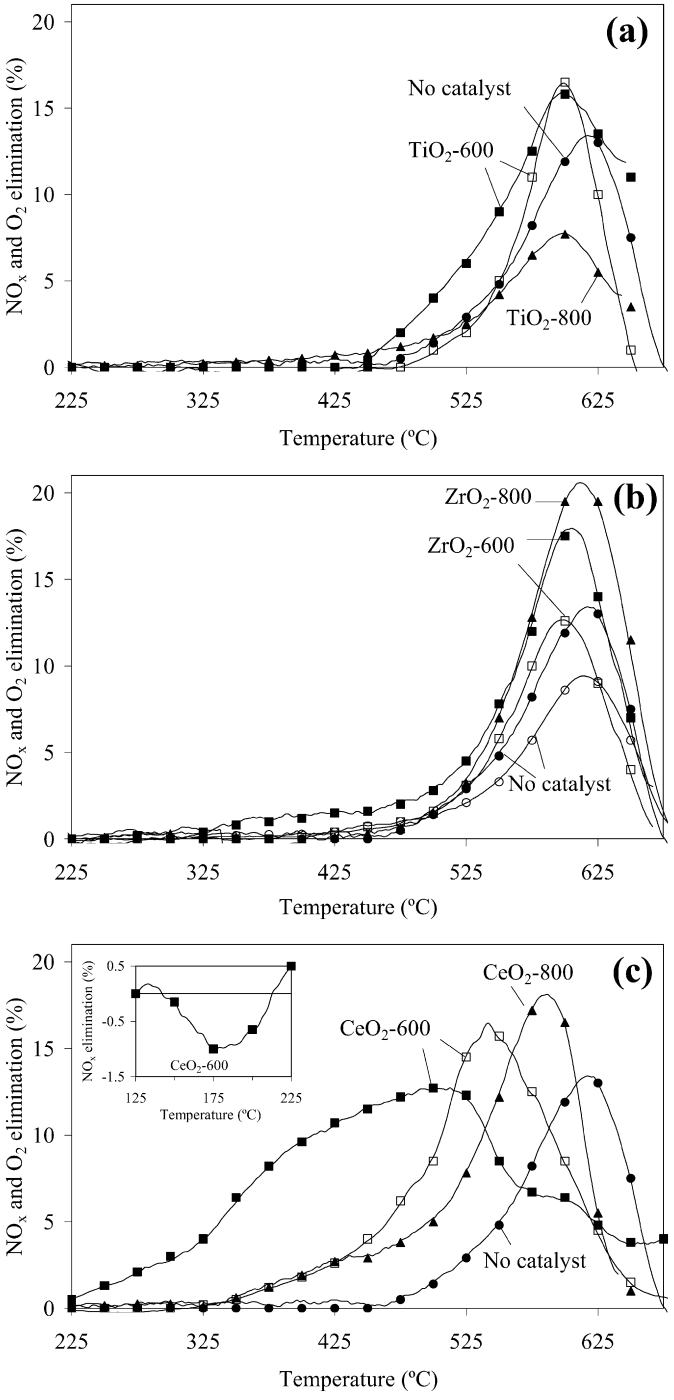


Fig. 4. $NO_x$ elimination in temperature programmed reactions under $NO_x/O_2$ (solid symbols) and $O_2$ elimination in some of these experiments (open symbols). Catalysts: (a) $TiO_2$, (b) $ZrO_2$, and (c) $CeO_2$.

The $CeO_2$-600 catalyst exhibited a unique behaviour, with $NO_x$ and $O_2$ elimination profiles not following parallel trends. As mentioned earlier, $NO_x$ elimination occurred within a wide range of temperatures, from ca. 225 °C to >700 °C. In contrast, the corresponding $O_2$ elimination curve exhibited a single peak between 325 and 700 °C. These differences between $O_2$ and $NO_x$ elimination profiles indicate that, in addition to the

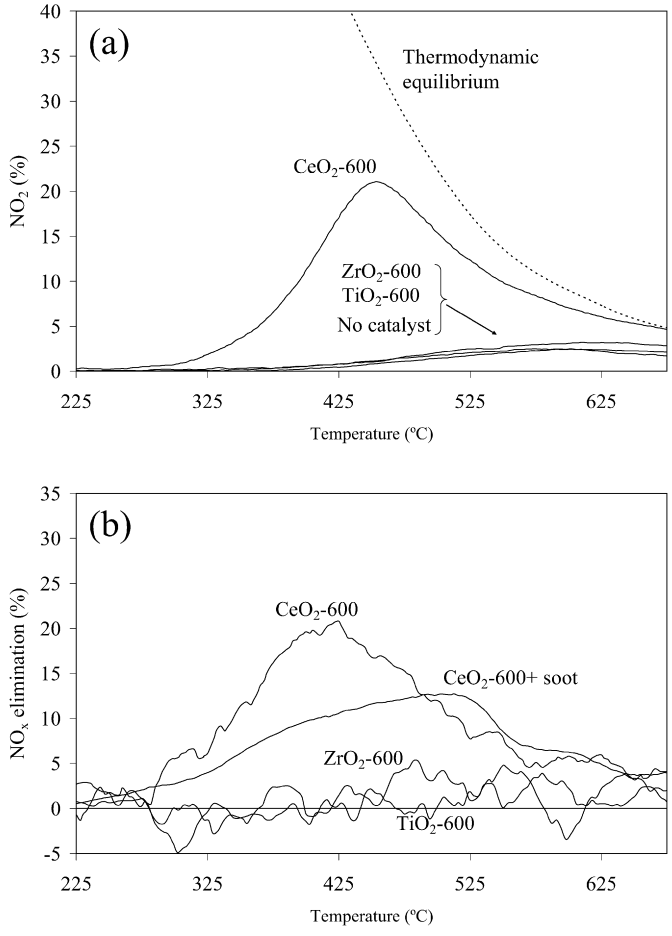


Fig. 5. Blank temperature programmed reactions (without soot) performed with catalysts calcined at 600 °C. (a) NO conversion to $NO_2$ and (b) $NO_x$ retention on catalysts. (The profile obtained with the catalyst $CeO_2$-600 from the soot oxidation experiment is included for comparison.)

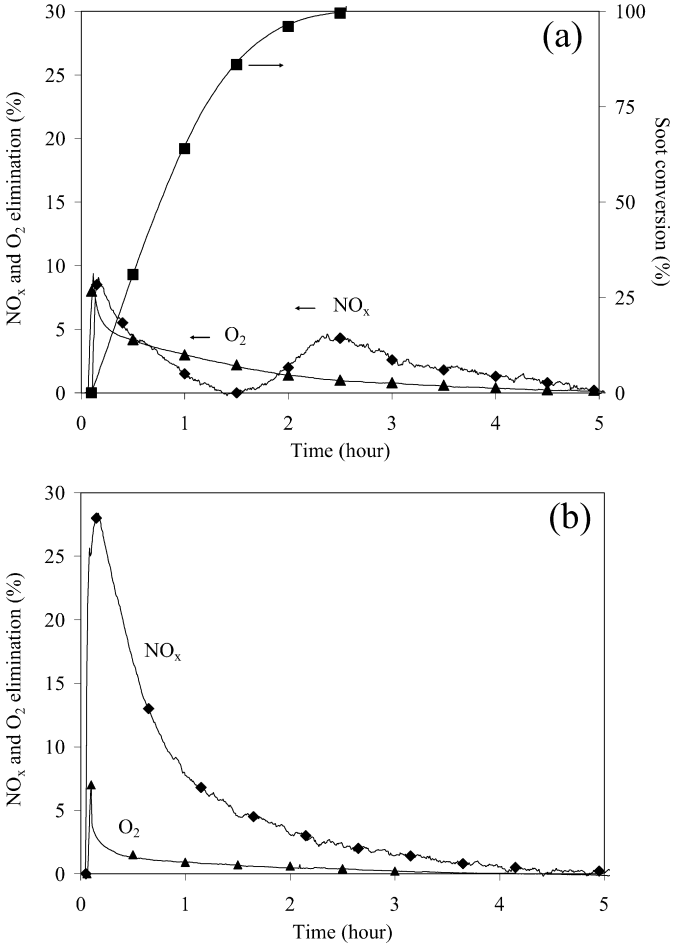


Fig. 6. Isothermal experiments at 450 °C under $NO_x/O_2$ performed with $CeO_2$-600: (a) catalysed soot oxidation and (b) blank experiment.

aforementioned $NO_x$ and $O_2$ reduction by soot at ca. 550 °C, an additional $NO_x$ elimination pathway was present at lower temperatures. Finally, note that a small amount of $NO_x$ was adsorbed on $CeO_2$-600 at room temperature, and then released between 150 and 200 °C, as shown on Fig. 4c.

In an attempt to provide some insight into the $NO_x$ elimination processes occurring in the catalysed soot oxidation experiments, we carried out blank TPRs (without soot) with the three catalysts calcined at 600 °C. The $NO_2$ percentage in the outlet gas mixture, calculated on the basis of the inlet $NO_x$ level, is plotted as a function of temperature in Fig. 5a, and the $NO_x$ elimination profiles are included in Fig. 5b. It is important to note that the $NO_2$ level in the gas stream is about zero at the entrance of the reactor, with NO being the main component of the $NO_x$ binary mixture. NO can be oxidised to $NO_2$ by $O_2$ according to

$$NO + 1/2O_2 \leftrightarrows NO_2. \quad (6)$$

The predicted $NO_2$ level considering the thermodynamic equilibrium of this reaction is represented in Fig. 5a as a dotted line.

$TiO_2$-600 and $ZrO_2$-600 exhibited no activity for $NO_2$ production, and the $NO_2$ level reached with these oxides is the same than that measured in the absence of catalyst (Fig. 5a). In the same way, the total concentration of $NO_x$ was constant throughout the experiments performed with these two oxides, and their $NO_x$ elimination profiles (included in Fig. 5b) exhibited the background level. In contrast, $CeO_2$-600 was quite effective for NO oxidation to $NO_2$ from 300 °C (Fig. 5a). The $NO_2$ profile obtained with this catalyst increased with temperature until the thermodynamic equilibrium of Eq. (6) was fulfilled, and then decreased at higher temperatures following thermodynamics. The highest $NO_2$ concentration was reached at 450 °C. This ability of $CeO_2$ in $NO_2$ production was reported previously [33]. In addition, $NO_x$ is stored on $CeO_2$-600 above ca. 250 °C, as shown in Fig. 5b. Physical adsorption of $NO_x$ can be ruled out in this temperature range, and chemical $NO_x$–$CeO_2$ interaction is expected. $NO_x$ desorption did not occur even though the catalyst was heated up to 700 °C. Fig. 5b also compiles the $NO_x$ elimination profile corresponding to the soot oxidation in TPRs performed with the $CeO_2$-600 (previously included in Fig. 4c). Surprisingly, $NO_x$ elimination decreased in the presence of soot with regard to the blank experiment.

Isothermal soot oxidation at 450 °C was performed under $NO_x/O_2$ with the $CeO_2$-600 catalyst, and a blank experiment (using the same catalyst but without soot) was performed under similar conditions. The soot conversion and $NO_x$ and $O_2$ elim-

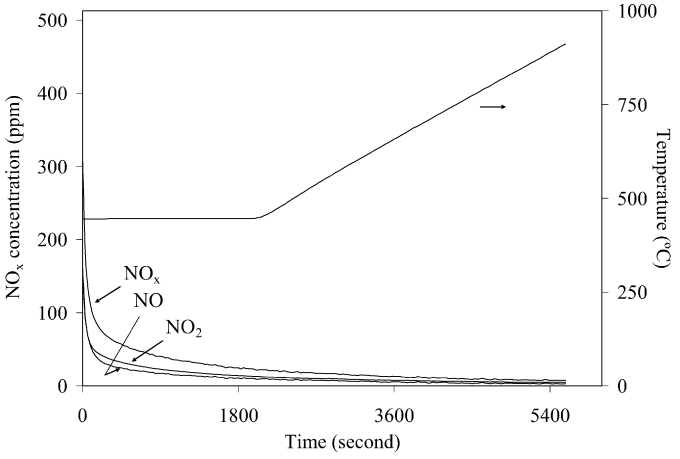


Fig. 7. Thermal treatment of $CeO_2$-600 under $N_2$ flow after the isothermal experiment at 450 °C under $NO_x/O_2$ (previously illustrated in Fig. 6b).

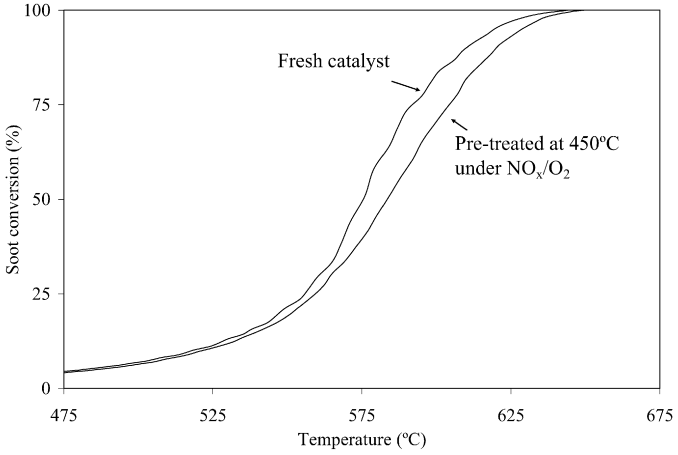


Fig. 8. $CeO_2$-600-catalysed soot oxidation by $O_2$ in temperature programmed reactions performed with fresh catalyst and with the pre-treated catalyst.

ination curves are illustrated in Fig. 6a, and those obtained in the blank experiment are shown in Fig. 6b. The soot conversion percentages (Fig. 6a) increased with time until total consumption, and both $NO_x$ and $O_2$ were eliminated from the gas stream during soot gasification. In this case, $CO_2$ was the only carbon product; CO emission was not detected. Special attention should be given to the $NO_x$ elimination curve, which showed two peaks, one appearing at the beginning of the soot oxidation experiment and the second appearing once the soot consumption was almost complete. In contrast, $O_2$ elimination reached a maximum level early and then decreased progressively until zero. Note that little $O_2$ elimination occurred after total soot conversion.

The $NO_x$ and $O_2$ elimination profiles were different in the blank experiment. In this case, a maximum elimination of both $NO_x$ and $O_2$ was reached after a few minutes, after which the levels progressively decreased to zero. The maximum $NO_x$ elimination level reached in the blank experiment exceeded the maximum level reached during the catalysed soot oxidation reaction, whereas the opposite situation was observed for the $O_2$ profiles.

Once the blank experiment was finished, the $NO_x/O_2$ mixture was replaced by $N_2$ and the temperature was raised up to 900 °C. As observed in Fig. 7, NO and $NO_2$ released, indicating that the previous $NO_x$ chemisorption is reversible and $NO_x$ stored on $CeO_2$-600 is further recovered under inert atmosphere (but not under $NO_x/O_2$, as mentioned).

Finally, after a blank experiment at 450 °C under $NO_x/O_2$ (similar to that included in Fig. 6b), the gas flow was replaced by $N_2$ and the furnace was cooled down quickly (after 20 min the temperature was below 250 °C). The gas composition was monitored during this time and evidences of emission of NO or $NO_2$ were not observed. Once the furnace reached room temperature, the $CeO_2$-600 was removed from the reactor and mixed with soot. A TPR was then performed with this pretreated catalyst using the gas mixture $O_2/N_2$. This experiment was done to determine the eventual contribution of the $NO_x$ species stored on the catalyst at 450 °C to the soot oxidation process.

Fig. 8 shows the soot conversion profile thus obtained, along with the curve corresponding to a similar experiment carried out with fresh catalyst. As can be deduced from Fig. 8, $NO_x$ stored on $CeO_2$ at 450 °C did not improve soot conversion, which occurred at even slightly higher temperature with the pretreated catalyst compared with the fresh catalyst.

## 4. Discussion

### 4.1. Comparison of $MO_2$ catalysts

It is generally known that surface area is of great importance in gas–solid catalysed reactions and that it becomes even more importantce in reactions in which catalyst (oxide) and one of the reactants (soot) must be in close contact. External surface area is the factor mainly responsible for the BET areas of the materials used in this study; thus, a relationship between surface area and particle size is common. For $CeO_2$, the results of the present study suggest that the relationship between the BET surface areas of $CeO_2$-600 and $CeO_2$-800 (37 and 6 $m^2/g$, respectively) and their catalytic activity ($T_{50\%} = 551$ and 581 °C, respectively) is not directly related to the soot-catalyst contact. As can be deduced from the catalytic tests, the high activity of $CeO_2$-600 for soot oxidation can be attributed to the conversion of NO to $NO_2$; for this reason, high surface area is preferable. Note that $NO_2$ had a much greater oxidizing effect than either NO or $O_2$. Calcination of $CeO_2$ at high temperature (800 °C) had a negative effect on its activity with regard to calcination at 600 °C due to sintering, thereby decreasing the BET surface area and also affecting some other properties of the oxide (e.g., oxygen storage capacity, oxygen mobility) that could be related to $NO_2$ production [33,34]. Calcination of $CeO_2$ at 800 °C also decreased its selectivity for $CO_2$ formation, instead of CO, as a soot oxidation product.

Despite the fact that a catalyst's BET surface area affects its catalytic activity, the nature of the catalyst is a more decisive factor than BET when $MO_2$ (M = Ti, Zr, Ce) oxides are compared. For instance, $CeO_2$-600, with 37 $m^2/g$, is much more active for soot oxidation than $TiO_2$-600 or $ZrO_2$-600, both with

47 $m^2/g$. This is because $CeO_2$ is able to catalyse the NO oxidation to $NO_2$, as mentioned, whereas $TiO_2$ and $ZrO_2$ are not.

The effect of calcination temperature on $TiO_2$ and $ZrO_2$ catalytic activity for soot oxidation is more complicated than that described for $CeO_2$. The phase composition of $TiO_2$ and $ZrO_2$ depends on the calcination temperature. Rutile phase is favoured for $TiO_2$ calcined at high temperature; monoclinic phase is favoured for $ZrO_2$ calcined at high temperature. Taking into account that the differences in catalytic activity of $TiO_2$-600 vs $TiO_2$-800 and $ZrO_2$-600 vs $ZrO_2$-800 are minor, it is possible to conclude that the phase composition does not play a crucial role on the activity of $TiO_2$ and $ZrO_2$ for soot oxidation. In the case of $TiO_2$, this observation was already reported [35]. Taking this idea into consideration, the minor differences in activity between $TiO_2$-600 and $TiO_2$-800 and between $ZrO_2$-600 and $ZrO_2$-800 could be attributed to the extent of soot-catalyst contact, which is related to their BET surface area. Because $TiO_2$ and $ZrO_2$ do not catalyse the NO oxidation to $NO_2$, the effect of surface area on this reaction can be ruled out.

With regard to $NO_x$ and $O_2$ elimination, both gases were consumed during the uncatalysed soot oxidation reaction. This process is not selective toward $NO_x$ reduction; above ca. 500 °C, $O_2$ oxidises soot to CO and $CO_2$, and $NO_x$ is reduced. TPRs followed by gas chromatography were performed without catalyst and with the $CeO_2$-600 catalyst; the results show that $N_2$ was the product of $NO_x$ reduction; formation of $N_2O$ was not observed. $TiO_2$ and $ZrO_2$ catalysts exhibited $O_2$ and $NO_x$ elimination profiles qualitatively similar to those observed in the uncatalysed process. $NO_x$ was reduced, along with a massive $O_2$ consumption above ca. 500 °C, indicating that these catalysts are not selective for $NO_x$ reduction by soot. The $NO_x$ elimination profiles obtained with the $CeO_2$ catalysts (mainly $CeO_2$-600 and, to a much lower extent, $CeO_2$-800) are quite different from those of $TiO_2$ and $ZrO_2$. Along with the aforementioned $NO_x$ reduction above 500 °C, another $NO_x$ elimination pathway occurred at lower temperature. We discuss this in detail in the next section.

Finally, an additional difference among the $MO_2$ catalysts studied here is the different selectivity for the formation of $CO_2$ instead of CO as the soot oxidation product. This can be seen in the data presented in Table 2. A general feature of carbon combustion reactions is that the CO/$CO_2$ ratio increases with temperature, because $CO_2$ is preferred at low temperature and CO is preferred at high temperature. Considering this idea, the highest selectivity of $CeO_2$-600 for $CO_2$ formation could be due on one hand to its highest activity for soot oxidation. $CeO_2$-600-catalysed soot combustion occurs in the lowest temperature range, and thus, CO formation is the lowest one. However, this general argument is not valid for explaining some of the data given in Table 2. For instance, $TiO_2$-600 and $ZrO_2$-600 had about the same $T_{50\%}$ value (593 and 592 °C, respectively), whereas their selectivity for $CO_2$ formation differed dramatically (CO = 56.6 and 43.4%, respectively). This is because of the differing activities of the catalysts in accelerating the reaction

$$CO + 1/2O_2 \rightarrow CO_2. \quad (7)$$

It is known that $CeO_2$ is a very effective catalyst for this reaction through oxidation using lattice oxygen [36]. The results obtained here suggest that $TiO_2$ is more active than $ZrO_2$ in catalysing reaction (7).

### 4.2. On the mechanism of $CeO_2$-catalysed $NO_x$-soot reaction

Depending on the reaction temperature, $CeO_2$ can participate in the $CeO_2$-catalysed $NO_x$-soot reaction mechanism in different ways. At low temperature, $CeO_2$ adsorbs $NO_x$, as can be deduced from the inset of Fig. 4c. It has been reported [32] that $NO_2$ stored at low temperature (200 °C [33]) can be decomposed at higher temperatures, and that the $NO_2$ thus evolved contributes to the accelerated oxidation of soot. But in a continuously regenerated soot trap, the temperature must be maintained above 200 °C; otherwise, soot is not converted to $CO_2$. Therefore, $NO_x$ storage at low temperature would not be expected to play a role in an actual trap.

At higher temperatures (above 250 °C), $CeO_2$ catalyses the oxidation of NO to $NO_2$ by Eq. (6), as shown in Fig. 5a. In the presence of soot, part of the $NO_2$ produced reacts with soot and part is chemisorbed on the oxide. The high efficiency of $CeO_2$ for $NO_2$ production is the main reason for the higher activity of this oxide for soot oxidation compared with $TiO_2$ or $ZrO_2$. The competition between $NO_2$ adsorption on $CeO_2$ and $NO_2$ reaction with soot can be clearly seen in Fig. 6. The amount of $NO_x$ eliminated at the beginning of the soot oxidation isothermal reaction at 450 °C (first peak of the $NO_x$ profile in Fig. 6a) was less than the amount of $NO_x$ eliminated in the absence of soot (Fig. 6b). In the presence of soot, part of the $NO_2$ produced by $CeO_2$ became NO due to soot oxidation and was not available for retaintion on $CeO_2$. However, once the soot was almost consumed, a second retention peak occurred (Fig. 6a), because although $NO_2$ consumption by soot no longer occurred to any great extent, the maximum $NO_x$ storage capacity of $CeO_2$ was not yet fulfilled. Another difference in behaviour among the three $MO_2$ oxides studied under $NO_x/O_2$ mixtures was the lack of $NO_x$ accumulation on $ZrO_2$ and $TiO_2$.

The $NO_x$ stored on $CeO_2$ during catalysed soot oxidation under a $NO_x$ or $O_2$ stream at 450 °C did not contribute to soot oxidation. As can be deduced from Fig. 8, the fresh $CeO_2$-600 for soot oxidation by $O_2$ and the same catalyst pretreated under $NO_x/O_2$ at 450 °C had about the same catalytic activity. In addition, the results obtained in this study do not demonstrate the amount of $NO_x$ stored on $CeO_2$ released under $NO_x/O_2$ atmosphere. This is supported by the fact that the $NO_x$ elimination profiles shown in Fig. 5b corresponding to $CeO_2$-600 did not reach negative values within the range of temperatures studied. The amount of $NO_x$ stored on $CeO_2$ only was released under a $NO_x$-free gas stream, as shown in Fig. 7, which includes $NO_x$ evolution profiles obtained under $N_2$.

## 5. Conclusions

Based on our comparison of the catalytic activity of $TiO_2$, $ZrO_2$, and $CeO_2$ for soot oxidation under $NO_x/O_2$, we can draw the following conclusions:

- $CeO_2$-600 is more active than $TiO_2$-600 and $ZrO_2$-600 for soot oxidation because it accelerates the conversion of NO to $NO_2$, whereas $TiO_2$ and $ZrO_2$ do not catalyse this reaction. The catalytic activity of all these three oxides decreases when calcined at 800 °C, with $CeO_2$ maintaining the highest activity among the three oxides studied despite the significant decrease in BET surface area.
- The phase composition of $TiO_2$ (rutile or anatase) and $ZrO_2$ (monoclinic or tetragonal) has no significant affect on the catalytic activity of these oxides. The main feature of these oxides that affects their activity is BET surface area, which may be related to better soot-catalyst contact.
- During $CeO_2$-catalysed soot oxidation, $NO_x$ is stored on this oxide. This is not the case for $TiO_2$- or $ZrO_2$-catalysed soot oxidation. However, $NO_x$ stored on $CeO_2$ does not accelerate soot oxidation. $NO_x$ stored on $CeO_2$ evolves subsequently under $N_2$ flow but not under $NO_x/O_2$ flow.
- During $CeO_2$-catalysed soot oxidation under $NO_x/O_2$, once $NO_2$ is produced by $CeO_2$, there is a competition between the $NO_2$-soot reaction and $NO_x$ storage on the catalyst.
- $CeO_2$-600 catalysed soot oxidation yields mainly $CO_2$, whereas $TiO_2$-600- and $ZrO_2$-600-catalysed soot oxidation yield higher percentages of CO. This additional benefit of $CeO_2$ compared with the other oxides can be explained considering two facts: (i) $CeO_2$-catalysed soot oxidation occurs at the lowest temperature, and (ii) $CeO_2$ catalyses the oxidation of CO to $CO_2$. $CeO_2$ calcination at 800 °C instead of 600 °C has a negative affect on the selectivity of this oxide toward $CO_2$ production.

## Acknowledgments

Financial support was provided by the Spanish Ministry of Education and Science (project CTQ2005-01358) and a contract of ABL (Ramon y Cajal Program), which is co-funded by the Generalitat Valenciana and the University of Alicante.

## References

[1] R.H. Hammerle, D.A. Ketcher, R.W. Horrocks, G. Lepperhoff, G. Hüthwohl, B. Lüers, SAE Technical Paper Series, Paper Number 942043, 1994.
[2] J.C. Summers, S. Van Houtte, D. Psaras, Appl. Catal. B 10 (1996) 139.
[3] J.H. Johnson, S.T. Bagley, L.D. Gratz, D.G. Leddy, SAE Technical Paper Series, Paper Number 940233, 1992.
[4] J. Oi-Uchisawa, S. Wang, T. Nanbaa, A. Ohi, A. Obuchi, Appl. Catal. B 44 (2003) 207.
[5] B.A.A.L. van Setten, J. Bremmer, S.J. Jelles, M. Makke, J.A. Moulijn, Catal. Today 53 (1999) 613.
[6] S. Biamino, P. Fino, D. Fino, N. Russo, C. Badini, Appl. Catal. B 61 (2005) 297.
[7] A. Bueno-López, K. Krishna, M. Makkee, J.A. Moulijn, Catal. Lett. 99 (2005) 203.
[8] A. Bueno-López, K. Krishna, M. Makkee, J.A. Moulijn, J. Catal. 230 (2005) 237.
[9] J. Oi-Uchisawa, A. Obuchi, R. Enomoto, S. Liu, T. Nanba, S. Kushiyama, Appl. Catal. B 26 (2000) 17.
[10] K. Villani, W. Vermandel, K. Smets, D. Liang, G. Van Tendeloo, J.A. Martens, Environ. Sci. Technol. 40 (2006) 2727.
[11] J.P.A. Neeft, O.P. van Pruissen, M. Makkee, J.A. Moulijn, Appl. Catal. B 12 (1997) 21.
[12] S. Braun, L.G. Appel, M. Schmal, Appl. Surf. Sci. 201 (2002) 227.
[13] M. Piacentini, M. Maciejewski, A. Baiker, Appl. Catal. B 72 (2007) 105.
[14] A. Kotsifa, D.I. Kondarides, X.E. Verykios, Appl. Catal. B 72 (2007) 136.
[15] J. van Doorn, J. Varloud, P. Meriaudeau, V. Perrichon, M. Chevrier, C. Gauthier, Appl. Catal. B 1 (1992) 117.
[16] J.P.A. Neeft, M. Makkee, J.A. Moulijn, Chem. Eng. J. 64 (1996) 295.
[17] E. Djurado, P. Bouvier, G. Lucazeau, J. Solid State Chem. 149 (2000) 399.
[18] B.-K. Kim, J.-W. Hahn, K.R. Han, J. Mater. Sci. Lett. 16 (1997) 669.
[19] L.D. Huy, P. Laffez, P. Daniel, A. Jouanneaux, N.T. Khoi, D. Simeone, Mater. Sci. Eng. B 104 (2003) 163.
[20] D.R. Clarke, J. Am. Ceram. Soc. 65 (1982) 284.
[21] M.S. Kaliszewski, G. Behrens, A.H. Heuer, M.C. Shaw, D.B. Marshall, G.W. Dransmanri, R.W. Steinbrech, A. Pajares, F. Guiberteau, F.L. Cumbrera, A. Dominguez-Rodriguez, J. Am. Ceram. Soc. 77 (1994) 1185.
[22] C. Su, B.Y. Hong, C.M. Tseng, Catal. Today 96 (2004) 119.
[23] R.A. Spurr, H. Myers, Anal. Chem. 29 (1957) 760.
[24] S.R. Dhage, V.D. Choube, V. Samuel, V. Ravi, Mater. Lett. 58 (2004) 2310.
[25] H. Cheng, J. Ma, Z. Zhao, L. Qi, Chem. Mater. 7 (1995) 663.
[26] S.P.S. Porto, P.A. Fleury, T.C. Daman, Phys. Rev. 154 (1967) 522.
[27] S.J. Rigby, A.H.R. Al-Obaidi, S.-K. Lee, D. McStay, P.K.J. Robertson, Appl. Surf. Sci. 252 (2006) 7948.
[28] L.A. Cortez-Lajas, J.M. Hernández-Enríquez, A. Castillo-Mares, J.L. Rivera-ARmetna, G. Sandoval-Robles, L.A. García-Serrano, R. García-Alamilla, Rev. Mexicana Ing. Quím. 5 (2006) 321.
[29] D. Michel, M. Perez, Y. Jorba, R. Collonges, J. Raman Spectrosc. 5 (1976) 163.
[30] L.N. Ikryannikova, A.A. Aksenov, G.L. Markaryan, G.P. Muraveva, B.G. Kostyuk, A.N. Kharlanov, E.V. Lunina, Appl. Catal. A 210 (2001) 225.
[31] A. Mineshige, T. Taji, Y. Muroi, M. Kobune, S. Fujii, N. Nishi, M. Inaba, Z. Ogumi, Solid State Ionics 135 (2000) 481.
[32] Y. Li, Q. Zhu, X. Zhang, B. Xu, J. Catal. 221 (2004) 584.
[33] A. Setiabudi, J. Chen, G. Mul, M. Makke, J.A. Moulijn, Appl. Catal. B 51 (2004) 9.
[34] E. Rocchini, A. Trovarelli, J. Llorca, G.W. Graham, W.H. Weber, M. Maciejewski, A. Baiker, J. Catal. 194 (2000) 461.
[35] I. Atribak, I. Such-Basáñez, A. Bueno-López, A. García-García, Catal. Commun. 8 (2007) 478.
[36] J. Kăspar, P. Fornasiero, M. Graziani, Catal. Today 50 (1999) 285.